FOKKER-PLANCK CALCULATIONS OF HOT-ELECTRON FORMATION BY ELECTRON CYCLOTRON RESONANCE HEATING IN THE TMX-UPGRADE TANDEM MIRROR

B.W. STALLARD, Y. MATSUDA, W.M. NEVINS
University of California,
Lawrence Livermore National Laboratory,
Livermore, California,
United States of America

ABSTRACT. The paper studies cold plasma trapping and heating of hot electrons in mirror geometry using a time-dependent, bounce-averaged Fokker-Planck code with quasi-linear diffusion due to RF heating at fundamental and second harmonic frequencies. With the restriction $k_{\parallel} = 0$, the code models the beam-controlled heating (spatially restricted electric fields) that will be used to create thermal barriers in the TMX-Upgrade tandem-mirror experiment. By spatially localizing the microwave beams, which are strongly absorbed in a single pass, the mean hot-electron energy may be controlled. Heating is away from the midplane to control anisotropy ($P_{\perp}/P_{\parallel}$). For a given magnetic field geometry and cold-plasma source temperature T_s, the parameters of the hot electrons scale with the quantity $\chi \equiv \epsilon^2/n_s\omega$, where ϵ is the electric field, n_s is the cold-plasma density, and ω is the frequency.

1. INTRODUCTION

Tandem-mirror devices with thermal barriers use electron cyclotron resonance heating (ECRH) to create the hot-electron populations in the barrier regions [1]. A comparison of the thermal barrier and the standard tandem configuration is illustrated in Fig.1. In the basic tandem mode [2] the confining potential is created by a plug-electron population n_p whose density exceeds a much larger volume centre-cell plasma of density n_c. With a uniform electron temperature T_e, the confining potential is given by a Boltzmann relation $\Phi_c = T_e \ln(n_p/n_c)$.

In the thermal-barrier mode, a depression in potential in the thermal barrier, created by a hot, mirror-trapped electron population, thermally isolates the plug electrons from the central-cell population. The confining potential can then be created for $n_p < n_c$ by using ECRH to heat plug electrons so that $T_{ep} > T_{ec}$. The reduced thermal contact between plug and centre-cell electrons makes this possible at modest ECRH power levels.

For the thermal-barrier mode the confining potential is given by [3]

$$\Phi_c \approx T_{ep} \ln\left[\frac{n_p}{n_b^*}\left(\frac{T_{ec}}{T_{ep}}\right)^{1/2}\right] - T_{ec} \ln\left(\frac{n_c}{n_b^*}\right) \qquad (1)$$

where subscripts p (c) for density and temperature refer to the plug (central cell). The quantity n_b^* is the passing density of central-cell electrons at the potential minimum in the barrier and equals the difference between the total density and the hot-electron density.

The reduced requirement on plug density to establish the confining potential significantly reduces the magnet and neutral beam technology constraints and the power requirements for the end plug of a tandem-mirror reactor compared with a standard tandem.

The tandem-mirror experiment, TMX-Upgrade, at Lawrence Livermore National Laboratory (LLNL) will employ ECRH to form thermal barriers and potential plugs in each end-cell [4]. The expected axial profiles of magnetic field, plasma potential and density are shown in Fig.2. The thermal barrier requires hot, mirror-trapped electrons of mean energy and density, $\bar{E}_{eh} \sim 50$ keV and $n_h < 5 \times 10^{12}$ cm^{-3}, respectively. To establish the barrier, a hot-to-passing density ratio $n_h/n_b^* \gg 1$ is necessary at the barrier potential minimum, see Eq.(1). In the potential plug the mean electron parameters are $T_{ep} \sim 1.4$ keV and $n_p \sim 7 \times 10^{12}$ cm^{-3}. For electron heating, four 200-kW, 28-GHz pulsed gyrotrons will be used, one at each heating location. Heating, using the extraordinary mode, is at the fundamental resonance in the potential peak and at the second harmonic in the barrier minimum.

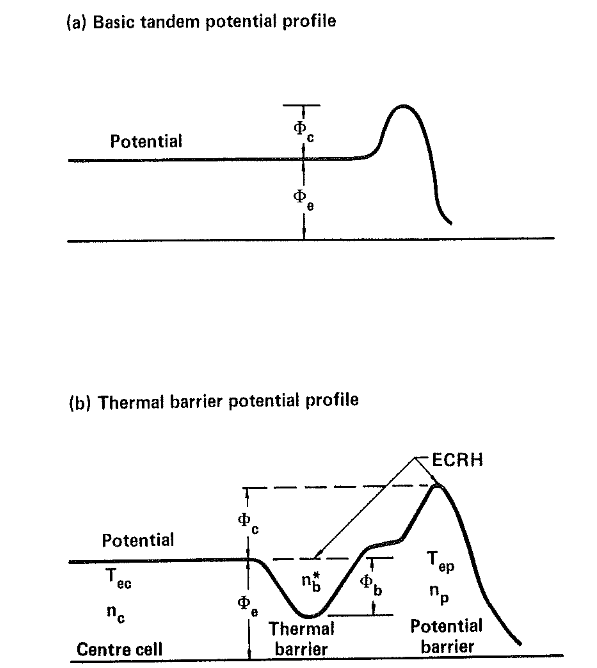

FIG.1. Comparison of axial potential profiles for the basic tandem and a tandem incorporating a thermal barrier. ECRH is used to create both the barrier and the plug potential, which confines centre-cell ions.

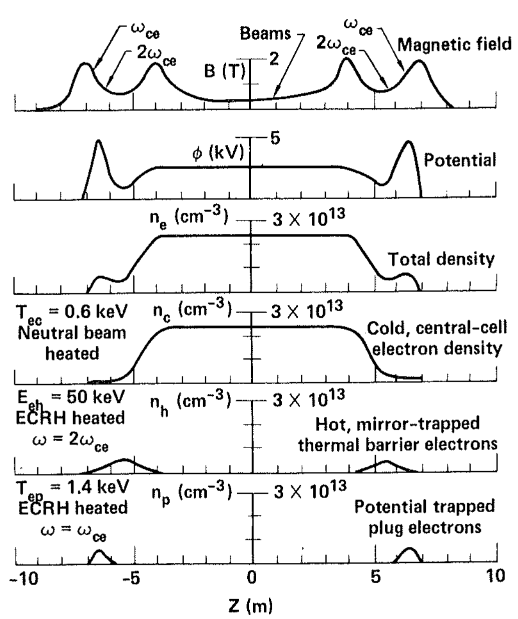

FIG.2. TMX-Upgrade axial profiles of magnetic field, plasma potential and electron density. Microwave power is applied in the end-cells to heat two distinct electron populations.

In Section 2 we discuss a scheme to control the hot-electron energy and anisotropy in the thermal barriers using localized electron heating. A Fokker-Planck code, which models the localized heating and calculates electron trapping and heating, is reviewed in Section 3. Results of the calculations are presented in Section 4. Finally, in Section 5 we summarize the conclusions of the calculations and indicate areas where further work is needed.

2. CONTROL OF HOT-ELECTRON ENERGY AND ANISOTROPY

2.1. Requirements on energy for the thermal barrier

It is necessary to control the mean energy of the hot-electron population in the thermal barrier cells of tandem mirrors. The magnitude of the required dip in the ambipolar potential, which forms the thermal barrier, is determined from the power balance of the plug-electron population. The required hot-electron density is in turn determined by the magnitude of this potential dip through the quasi-neutrality condition. Magnetohydrodynamic (MHD) stability sets a limit on the hot-electron pressure. At fixed density, this constraint can be satisfied only by limiting the mean energy of the hot-electron population. This limiting temperature is about 50 keV in TMX-Upgrade.

The mean energy observed in several experiments using ECRH in either single or linked mirrors (bumpy tori) [5] obeys a non-adiabatic scaling law [6] $\rho/L_B \cong 0.05$, where ρ is the gyroradius of the hot electrons and L_B is the magnetic field scale length. For TMX-Upgrade ($L_B \cong 1$ m) this scaling law predicts a mean energy for the hot-electron population of the order of 10 MeV. Although other loss processes (e.g. synchrotron radiation) would limit the mean energy below 10 MeV, clearly it will be necessary to control the mean energy of the hot-electron population in TMX-Upgrade by some other mechanism.

We believe that the mean energy of the hot-electron population can be limited, as required for the TMX-Upgrade tandem mirror, by localized heating with strong single-pass absorption. The experiments considered in Ref.[5] all employed cavity heating; i.e. there was a significant amplitude in the heating field at all spatial locations and hence over the entire range of magnetic field amplitudes within the plasma. In TMX-Upgrade the microwave beam will be well collimated axially. In tandem-mirror geometry the

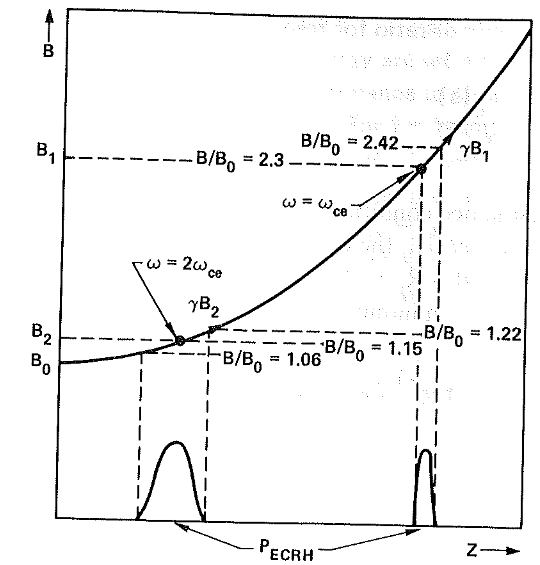

FIG.3. Illustration of a method to control hot-electron energy in the thermal barrier through the use of localized heating. The resonance for hot electrons shifts to higher magnetic field where the RF electric field is weaker.

dominant magnetic field gradients are axial (rather than radial as in tokamak geometry) [7]. Hence, by limiting the axial extent of the radially propagating microwave beam, as shown in Fig.3, the hot electrons will become 'detuned' from the cyclotron resonance as their energy becomes mildly relativistic. As the relativistic mass increase shifts the resonance axially to higher magnetic fields where the RF field is much weaker, the heating rate will strongly decrease and the maximum electron energy will be limited.

Control of hot-electron anisotropy, important for microinstability [8], is also possible by varying the mirror ratio for off-midplane heating. In TMX-Upgrade the mirror ratio for heating in the thermal barrier can be varied by means of movable microwave horns whose aiming along the magnetic axis can be adjusted. Resonance is maintained by simultaneous adjustment of the magnetic field.

2.2. Penetration and absorption of the microwave power

The ability to control energy by resonance detuning is sensitive to the parallel index of refraction, $N_\parallel = k_\parallel c/\omega$, of the waves, since the Doppler shift, as well as the relativistic mass increase, affects the absorption profile.

Ray-tracing calculations in the TMX-Upgrade mirror geometry have been carried out for the extra-ordinary mode at the fundamental and second harmonics. At the second harmonic, ray bending is small if the plasma density is not too close to cut-off. An example of this is shown in Fig.4. The $N_\parallel$ spectrum is largely determined by the angle of beam aiming and the divergence of the microwave beam. Small $N_\parallel$ (which is important for energy control) is obtained by

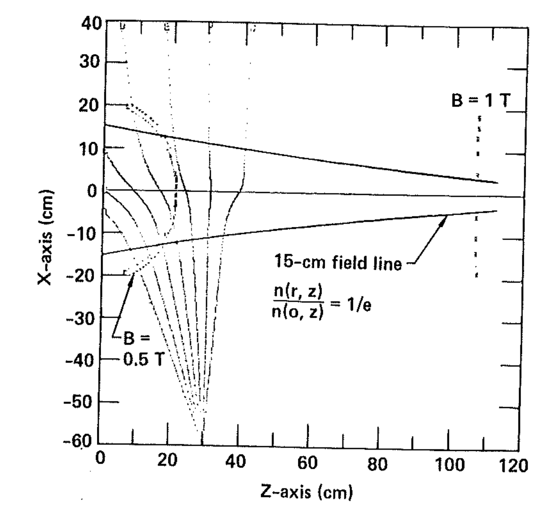

FIG.4. Ray-tracing calculations in the thermal barrier for TMX-Upgrade, for a beam aiming near normal to the magnetic axis (extraordinary mode, $\omega = 2\omega_{ce}$). The midplane peak density is 4.1×10^{12} cm^{-3}.

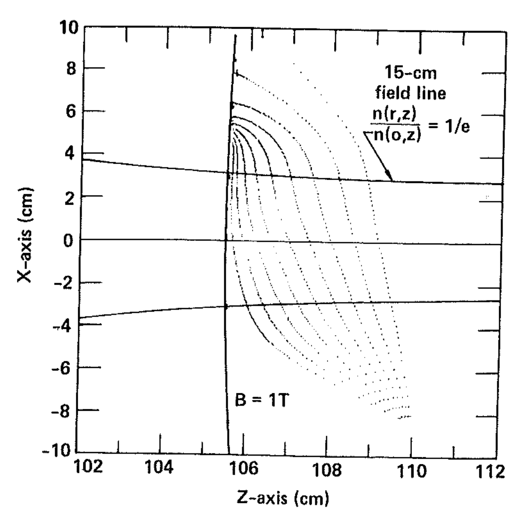

FIG.5. Ray-tracing calculation at the potential peak in TMX-Upgrade (extraordinary mode, $\omega = \omega_{ce}$). The maximum plug density is 7×10^{12} cm^{-3}.

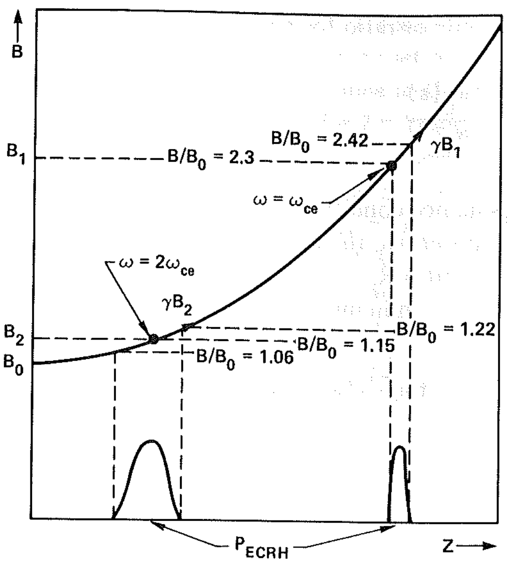

FIG.3. Illustration of a method to control hot-electron energy in the thermal barrier through the use of localized heating. The resonance for hot electrons shifts to higher magnetic field where the RF electric field is weaker.

dominant magnetic field gradients are axial (rather than radial as in tokamak geometry) [7]. Hence, by limiting the axial extent of the radially propagating microwave beam, as shown in Fig.3, the hot electrons will become 'detuned' from the cyclotron resonance as their energy becomes mildly relativistic. As the relativistic mass increase shifts the resonance axially to higher magnetic fields where the RF field is much weaker, the heating rate will strongly decrease and the maximum electron energy will be limited.

Control of hot-electron anisotropy, important for microinstability [8], is also possible by varying the mirror ratio for off-midplane heating. In TMX-Upgrade the mirror ratio for heating in the thermal barrier can be varied by means of movable microwave horns whose aiming along the magnetic axis can be adjusted. Resonance is maintained by simultaneous adjustment of the magnetic field.

2.2. Penetration and absorption of the microwave power

The ability to control energy by resonance detuning is sensitive to the parallel index of refraction, $N_{\parallel} = k_{\parallel} c/\omega$, of the waves, since the Doppler shift, as well as the relativistic mass increase, affects the absorption profile.

Ray-tracing calculations in the TMX-Upgrade mirror geometry have been carried out for the extraordinary mode at the fundamental and second harmonics. At the second harmonic, ray bending is small if the plasma density is not too close to cut-off. An example of this is shown in Fig.4. The $N_{\parallel}$ spectrum is largely determined by the angle of beam aiming and the divergence of the microwave beam. Small $N_{\parallel}$ (which is important for energy control) is obtained by

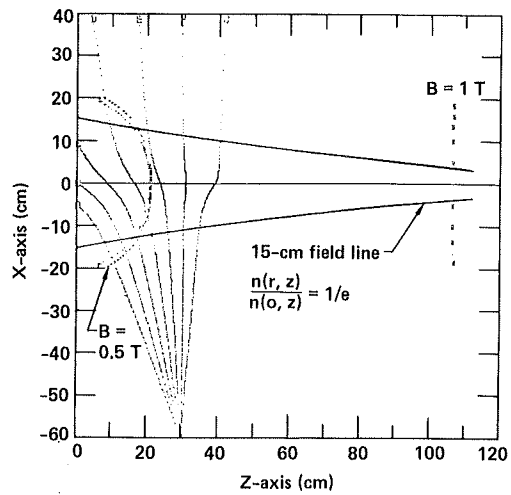

FIG.4. Ray-tracing calculations in the thermal barrier for TMX-Upgrade, for a beam aiming near normal to the magnetic axis (extraordinary mode, $\omega = 2\omega_{ce}$). The midplane peak density is 4.1×10^{12} cm^{-3}.

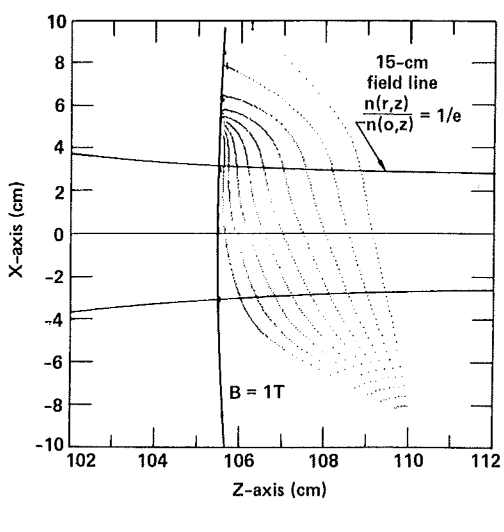

FIG.5. Ray-tracing calculation at the potential peak in TMX-Upgrade (extraordinary mode, $\omega = \omega_{ce}$). The maximum plug density is 7×10^{12} cm^{-3}.

aiming the microwave beam as near normal as possible to the magnetic field lines. In addition, theory predicts maximum wave absorption at normal incidence for the extraordinary mode [9]. For TMX-Upgrade parameters, total absorption in a single pass is expected.

On the other hand, for the extraordinary mode at the fundamental harmonic, strong ray bending and large $N_\parallel$ ($\sim$ 1) is predicted for mirror geometry (see Porkolab et al. [9] and Batchelor et al. [10]). A ray-tracing example for TMX-Upgrade is shown in Fig.5. Absorption theory for the high-density regime ($\omega_{pe}^2/\omega_{ce}^2 > 2(v_t/c)^2$, where v_t is the electron thermal velocity and ω_{pe}, ω_{ce} have their usual definitions) predicts total single-pass attenuation for large $N_\parallel$ at TMX-Upgrade parameters (see Ref.[9]). This contrasts with the theoretical prediction of very weak absorption as $N_\parallel \to 0$ which results from a 'shorting out' of the RF electric field by the plasma dielectric field [11].

The Fokker-Planck calculations, which are presented in Section 4, were calculated with a model for which $N_\parallel = 0$. Since the electric field is an input parameter for the code, the weak absorption result predicted by theory does not arise in the code. However, to support the assumption of the code that heating may be limited at the fundamental harmonic when $N_\parallel$ is not small, we must examine the sensitivity to $N_\parallel$ of the localized heating scheme.

2.3. Resonance for $N_\parallel = 0$

The resonance condition for trapped electrons in the spatially dependent magnetic field of mirror geometry is

$$\frac{\ell\,\omega_c(s)}{\gamma} = \omega\left(1 - N_\parallel \frac{v_\parallel(s)}{c}\right) \tag{2}$$

where ℓ is the harmonic number, $\omega_c(s) = eB(s)/m$ is the 'cold' electron cyclotron resonance frequency, ω is the applied frequency, s is the distance measured from the magnetic minimum (well bottom), and $\gamma = [1-(v/c)^2]^{-1/2}$ is the relativistic mass coefficient.

We note that the electron parallel velocity in a mirror, $v_\parallel$, is a function of position s. For spatially limited (in s) RF electric fields, Eq.(2) determines the ranges of energy where resonance is possible.

We first consider the simplest case, $N_\parallel = 0$. Setting $N_\parallel = 0$ in Eq.(2) and defining

$$R_\mu \equiv \frac{\omega}{\omega_c(0)}$$

and the mirror ratio for resonance

$$R_\rho(s) \equiv \frac{\omega_c(s)}{\omega_c(0)}$$

the resonance condition is $R_\rho = \gamma R_\mu/\ell$. Neglecting plasma potential, the condition for resonance to occur at mirror ratio R_ρ is that the electron pitch angle at the magnetic minimum, θ_0, must satisfy

$$\theta_{\ell c} \le \theta_0 \le \tan^{-1}\left\{R_\rho - 1\right\}^{-1/2} = \tan^{-1}\left\{\frac{\gamma R_\mu}{\ell} - 1\right\}^{-1/2} \tag{3}$$

The upper bound on θ_0 is the turning point resonance curve, and this satisfies the condition that the electron mirrors at a large enough mirror ratio to reach the resonance. However, if θ_0 exceeds the loss-cone angle given by $\theta_{\ell c} = \tan^{-1}(R_M - 1)^{-1/2}$, where R_M is the maximum mirror ratio, the electron is no longer confined. Thus, an energy-dependent range of θ_0, given by Eq.(3), determines the pitch angle for possible resonance. For resonance to occur, however, the RF electric field must be non-zero. Therefore, the mirror ratio range, $[R_\rho]$, of the non-zero RF field determines the θ_0, v_0 phase space region where resonance can occur.

An illustrative example is the resonance plot for $R_\mu = 2.3$ shown in Fig.6. The electric field is assumed localized in the regions $[R_\rho]_1$: $2.3 \leqslant R_\rho \leqslant 2.42$; $[R_\rho]_2$: $1.06 \leqslant R_\rho \leqslant 1.22$. A mirror ratio R = 4 sets the loss-cone angle $\theta_{\ell c} = 30°$.

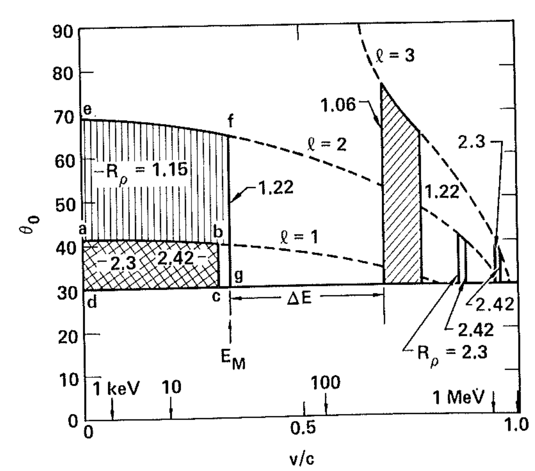

FIG.6. Resonance plot in midplane velocity space for RF electric field restricted to $1.06 \leqslant R_\rho \leqslant 1.22$ and $2.3 \leqslant R_\rho \leqslant 2.42$, for the case $N_\parallel = 0$ and $R_\mu = 2.3$. The fundamental harmonic and two harmonics are shown. The energy limit E_M and energy gap ΔE are indicated.

The resonance regions for $\ell = 1,2,3$ are shown. The upper and lower bounds in energy are set by the relativistic mass shift of the resonance to the boundaries of the localized electric fields. For $\ell = 1$, the boundary line labelled a-d at zero velocity ($\gamma = 1$) occurs at the resonance mirror ratio $R_\rho = 2.3$; i.e. the magnetic field for 'cold plasma' resonance, $\omega = \omega_{ce}$. The upper energy boundary, line b-c, occurs at $R_\rho = 2.42$. Similar energy boundaries for $\ell = 2$ and $\ell = 3$ are indicated in the figure. The boundary line e-d at zero velocity for $\ell = 2$ occurs at $R_\rho = 1.15$ ('cold plasma' resonance, $\omega = 2\omega_{ce}$), rather than the lower boundary of the RF field at $R_\rho = 1.06$, since resonance at lower magnetic fields for $N_\parallel = 0$ and $\ell = 2$ does not occur.

At sufficiently high energy, the curves show that $\ell = 2$ resonance is possible at the position of fundamental resonance for cold electrons and that $\ell = 3$ resonance occurs within both localized regions. We note that resonance at $\ell = 2$ terminates at a cut-off energy $E_M = 31$ keV and that an energy gap $\Delta E = 164$ keV exists between $\ell = 2$ and $\ell = 3$ resonances. This gap should effectively limit the average electron energy below E_M.

2.4. Resonance for $N_\parallel \neq 0$

The situation for non-zero $N_\parallel$ is more complex. Given the magnetic field for resonance, $\omega_c(s)$, as determined from the RF electric fields, Eq.(2) defines the parallel velocity of resonant electrons. It follows from energy conservation and the adiabatic invariance of the magnetic moment that the magnetic minimum phase space co-ordinates, $v_\perp(0)$ and $v_\parallel(0)$, of the resonant electrons can be found from $v_\parallel(s)$, from the axial profiles of magnetic field, and from plasma potential. Neglecting plasma potential, the parallel velocity as a function of s and the well-bottom pitch angle θ_0 is

$$v_\parallel(s) = v(1 - R_\rho(s)\sin^2\theta_0)^{1/2} \tag{4}$$

Inserting Eq.(4) into Eq.(2), the resonance condition for θ_0 reduces to

$$\theta_0 = \sin^{-1}\left\{\frac{1}{R_\rho}\left[1 - \frac{1}{(\gamma^2-1)}\left(\frac{R_\rho - \gamma\frac{R_\mu}{\ell}}{N_\parallel\frac{R_\mu}{\ell}}\right)^2\right]\right\}^{1/2} \tag{5}$$

Thus, given $N_\parallel$, ℓ, R_μ and R_ρ, the electron pitch angle satisfying resonance is determined as a function of energy (γ).

An example of $\ell = 2$ resonance for several values of $N_\parallel$ is shown in Fig.7 for resonance at $R_\rho = 1.22$, the same upper boundary of the localized RF field in $[R_\rho]_2$ as assumed for the plot of Fig.6. The solid line f-g shows resonance at $N_\parallel = 0$. As $N_\parallel$ increases (dotted lines), Doppler broadening splits the $N_\parallel = 0$ line into two resonance lines, f-g$^+$ and f-g$^-$, corresponding to the two signs of $v_\parallel$ as the electron oscillates axially in the magnetic well. The curves labelled +(−) correspond to anti-parallel (parallel) electron and wave phase velocities. The minus branch of the resonance line moves to greater energy as $N_\parallel$ increases.

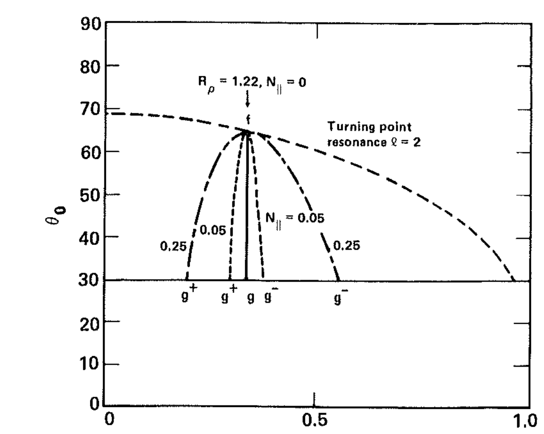

FIG.7. Plot showing line splitting of the resonance as $N_\parallel$ is increased from zero for resonance at a mirror ratio $R_\rho = 1.22$.

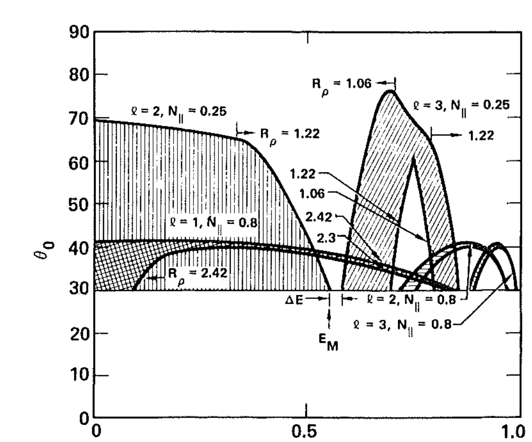

FIG.8. Resonance plot for non-zero $N_\parallel$ for the same parameters as assumed in Fig.6, except that $N_\parallel = 0.25$ for $1.06 \leqslant R_\rho \leqslant 1.22$ and $N_\parallel = 0.8$ for $2.3 \leqslant R_\rho \leqslant 2.42$.

The resonance regions for $\ell = 1,2,3$ are shown. The upper and lower bounds in energy are set by the relativistic mass shift of the resonance to the boundaries of the localized electric fields. For $\ell = 1$, the boundary line labelled a-d at zero velocity ($\gamma = 1$) occurs at the resonance mirror ratio $R_\rho = 2.3$; i.e. the magnetic field for 'cold plasma' resonance, $\omega = \omega_{ce}$. The upper energy boundary, line b-c, occurs at $R_\rho = 2.42$. Similar energy boundaries for $\ell = 2$ and $\ell = 3$ are indicated in the figure. The boundary line e-d at zero velocity for $\ell = 2$ occurs at $R_\rho = 1.15$ ('cold plasma' resonance, $\omega = 2\omega_{ce}$), rather than the lower boundary of the RF field at $R_\rho = 1.06$, since resonance at lower magnetic fields for $N_\parallel = 0$ and $\ell = 2$ does not occur.

At sufficiently high energy, the curves show that $\ell = 2$ resonance is possible at the position of fundamental resonance for cold electrons and that $\ell = 3$ resonance occurs within both localized regions. We note that resonance at $\ell = 2$ terminates at a cut-off energy $E_M = 31$ keV and that an energy gap $\Delta E = 164$ keV exists between $\ell = 2$ and $\ell = 3$ resonances. This gap should effectively limit the average electron energy below E_M.

2.4. Resonance for $N_\parallel \neq 0$

The situation for non-zero $N_\parallel$ is more complex. Given the magnetic field for resonance, $\omega_c(s)$, as determined from the RF electric fields, Eq.(2) defines the parallel velocity of resonant electrons. It follows from energy conservation and the adiabatic invariance of the magnetic moment that the magnetic minimum phase space co-ordinates, $v_\perp(0)$ and $v_\parallel(0)$, of the resonant electrons can be found from $v_\parallel(s)$, from the axial profiles of magnetic field, and from plasma potential. Neglecting plasma potential, the parallel velocity as a function of s and the well-bottom pitch angle θ_0 is

$$v_\parallel(s) = v(1 - R_\rho(s)\sin^2\theta_0)^{1/2} \tag{4}$$

Inserting Eq.(4) into Eq.(2), the resonance condition for θ_0 reduces to

$$\theta_0 = \sin^{-1}\left\{\frac{1}{R_\rho}\left[1 - \frac{1}{(\gamma^2 - 1)}\left(\frac{R_\rho - \gamma\frac{R_\mu}{\ell}}{N_\parallel\frac{R_\mu}{\ell}}\right)^2\right]\right\}^{1/2} \tag{5}$$

Thus, given $N_\parallel$, ℓ, R_μ and R_ρ, the electron pitch angle satisfying resonance is determined as a function of energy (γ).

An example of $\ell = 2$ resonance for several values of $N_\parallel$ is shown in Fig.7 for resonance at $R_\rho = 1.22$, the same upper boundary of the localized RF field in $[R_\rho]_2$ as assumed for the plot of Fig.6. The solid line f-g shows resonance at $N_\parallel = 0$. As $N_\parallel$ increases (dotted lines), Doppler broadening splits the $N_\parallel = 0$ line into two resonance lines, f-g$^+$ and f-g$^-$, corresponding to the two signs of $v_\parallel$ as the electron oscillates axially in the magnetic well. The curves labelled +(−) correspond to anti-parallel (parallel) electron and wave phase velocities. The minus branch of the resonance line moves to greater energy as $N_\parallel$ increases.

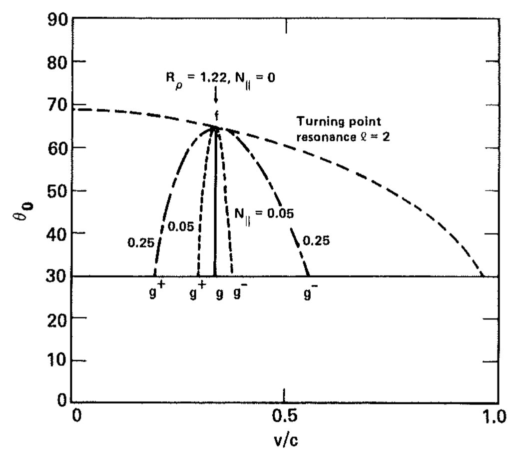

FIG.7. Plot showing line splitting of the resonance as $N_\parallel$ is increased from zero for resonance at a mirror ratio $R_\rho = 1.22$.

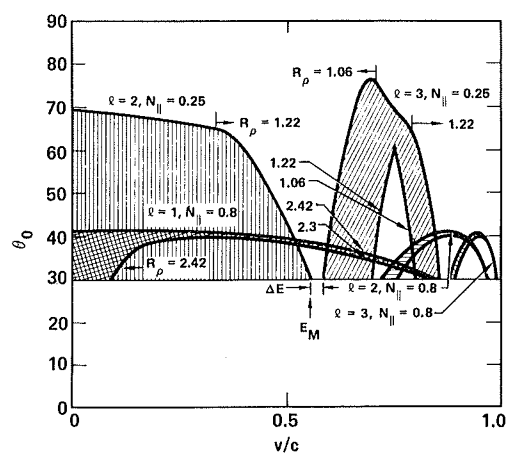

FIG.8. Resonance plot for non-zero $N_\parallel$ for the same parameters as assumed in Fig.6, except that $N_\parallel = 0.25$ for $1.06 \leqslant R_\rho \leqslant 1.22$ and $N_\parallel = 0.8$ for $2.3 \leqslant R_\rho \leqslant 2.42$.

The resonance plot for the same parameters as assumed in Fig.6, but with non-zero $N_\parallel$, is shown in Fig.8. Each resonance area of Fig.6 ($N_\parallel = 0$), as transformed by non-zero $N_\parallel$, is shown in Fig.8 with the same shading. The assumed values for the parallel index are $N_\parallel = 0.8$ for $[R_\rho]_1$ and $N_\parallel = 0.25$ for $[R_\rho]_2$. These values are averages determined from ray-tracing calculations. The value $N_\parallel = 0.25$ includes the finite beam width of the horns in the thermal barrier region and assumes horn-aiming perpendicular to the magnetic axis.

Several boundaries of the resonance regions are determined by distinct values of R_ρ as indicated. Other portions of the boundary are determined by the envelope of Doppler-split resonance lines of the type shown in Fig.7. Comparing the non-zero $N_\parallel$ plot with the case $N_\parallel = 0$, the effects of line splitting are evident. There is also an increase in E_M to $E_M = 101$ keV and a reduction of the energy gap ΔE to $\Delta E = 16$ keV. An important effect of large $N_\parallel$ is a significant narrowing of the resonance width in pitch angle for the $\ell = 1$ resonance at high energy. Although this 'resonance bridge' joins the $\ell = 2$ and $\ell = 3$ resonances, the narrowness of the bridge should strongly reduce the diffusion to higher energy since an electron may angle-scatter out of resonance before undergoing large energy increases. Preliminary Monte-Carlo calculations modelling these effects for TMX-Upgrade parameters support this conclusion [12].

3. FOKKER-PLANCK CODE

For the present study, we have modified an existing bounce-averaged Fokker-Planck code written by Cutler et al. [13] to suit our purpose, the major modification being the addition of quasi-linear RF diffusion terms due to ECRH. The code follows the evolution of a distribution function $f(v_0, \theta_0, t)$ at the midplane of a magnetic well, where v_0 and θ_0 are speed and pitch angle of a particle when it passes the midplane. The distribution function at any axial position can be obtained from $f(v_0, \theta_0, t)$ by particle orbit equations.

The axial profile of the magnetic field is assumed to be symmetric about the midplane. We assume zero ambipolar potential in the present study. A non-linear collision operator is used for electron-electron collisions. Electron-ion collisions are treated linearly, i.e. ions are fixed and contribute to pitch-angle scattering only.

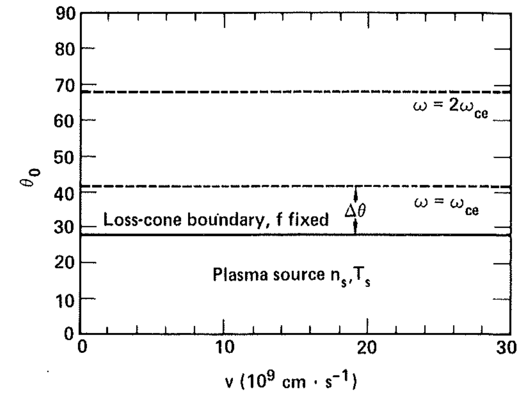

FIG.9. Midplane (magnetic minimum) velocity space for the Fokker-Planck code showing resonance lines and imposed boundary conditions.

The midplane (field minimum) velocity space is depicted in Fig.9. The particle source for mirror-trapped electrons is a low-temperature Maxwellian plasma source of density n_s and temperature T_s that fills the loss cone. Electrons become trapped at low energy by both collisions and RF diffusion across the loss-cone boundary. Both processes determine losses into the loss cone over the entire energy range and across a $v_0 = v_{max}$ boundary.

The quasi-linear diffusion terms added can be obtained, for example, by bounce-averaging a local quasi-linear equation

$$\left(\frac{\partial f}{\partial t}\right)_{QL} = \frac{1}{v_\perp}\frac{\partial}{\partial v_\perp}\left(v_\perp D \frac{\partial f}{\partial v}\right) \tag{6}$$

where $v_\perp$ is the perpendicular velocity and D is the quasi-linear diffusion coefficient. The diffusion coefficient is given by

$$D = \sum_\ell \frac{\pi e^2}{8 m^2} \epsilon^2 \delta(\omega - \ell\omega_c) J_{\ell-1}^2 \left(\frac{k_\perp v_\perp}{\omega_c}\right) \tag{7}$$

where J_ℓ is a Bessel function of order ℓ and the other quantities have their usual definitions. It is assumed that $k_\parallel = 0$ and that only the right-hand polarized electric field, $\epsilon \equiv |E_x - iE_y|$, is non-zero. In Eq.(7), ϵ and ω_c are taken to be dependent on the axial position, s, or, equivalently, the mirror ratio $R_\rho = B(s)/B(0)$.

The result may be written in a conservative form

$$\left\langle\left(\frac{\partial f}{\partial t}\right)_{QL}\right\rangle = \left(\frac{1}{\tau}\right)\frac{1}{2\pi v_0^3 \sin\theta_0 \cos\theta_0} \times \left[\frac{\partial}{\partial v_0}\left(D_{vv}\frac{\partial f}{\partial v_0} + D_{v\theta}\frac{\partial f}{\partial \theta_0}\right) + \frac{\partial}{\partial \theta_0}\left(D_{v\theta}\frac{\partial f}{\partial v_0} + D_{\theta\theta}\frac{\partial f}{\partial \theta_0}\right)\right] \tag{8}$$

where the brackets denote the bounce average, $\tau = \oint ds/|v_\parallel|$ is the bounce time, and the diffusion coefficients are given by

$$D_{vv} = \oint \frac{ds}{|v_\parallel|} 2\pi v_0^3 \sin^3\theta_0 \cos\theta_0 D$$

$$D_{v\theta} = \oint \frac{ds}{|v_\parallel|} 2\pi v_0^2 \sin^2\theta_0 \left(\frac{1 - R_\rho \sin^2\theta}{R_\rho}\right) D$$

$$D_{\theta\theta} = \oint \frac{ds}{|v_\parallel|} 2\pi v_0 \tan\theta_0 \left(\frac{1 - R_\rho \sin^2\theta_0}{R_\rho}\right)^2 D$$

Note that we have used a non-relativistic form of the quasi-linear equation. To include the effects of the relativistic resonance shift, we replace $\delta(\omega - \ell\omega_c)$ by $\delta(\omega - \ell\omega_c/\gamma)$ in Eq.(7), where γ is the mass factor defined earlier. Then, the Fokker-Planck equation to be solved is

$$\frac{\partial f}{\partial t} = \left\langle\left(\frac{\partial f}{\partial t}\right)_{cc}\right\rangle + \left\langle\left(\frac{\partial f}{\partial t}\right)_{QL}\right\rangle \tag{9}$$

where $\langle(\partial f/\partial t)_{cc}\rangle$ represents the bounce-averaged form of the non-linear Coulomb collision terms [13]. The boundary conditions employed are $f(v_0, \theta_{\ell c}, t) = n_s g_s(v_0)$ (i.e. fixed by a plasma source at the loss-cone boundary $\theta_0 = \theta_{\ell c}$; $f(v_{max}, \theta_0, t) = 0$ (i.e. absorbing boundary at $v = v_{max}$, normally taking the velocity of light as v_{max}); and $f(v_0, \pi/2, t)$ being regular).

Defining $f(v, \theta) \equiv n_s f'(v, \theta, t)$ we note that for the non-linear collision term $(\partial f/\partial t)_{cc} = n_s^2 (\partial f'/\partial t)_{cc}$. Performing the bounce average, the steady-state equation can be formally written as

$$0 = \pi \frac{e}{2m} \sum_\ell^2 \frac{\epsilon_\ell^2}{n_s}\left\langle\frac{1}{v_\perp}\frac{\partial}{\partial v_\perp} \times \left[v_\perp \delta\left(\omega - \frac{\ell\omega_c}{\gamma}\right) J_{\ell-1}^2\right]\frac{\partial f'}{\partial v_\perp}\right\rangle - \left\langle\left(\frac{\partial f'}{\partial t}\right)_{cc}\right\rangle \tag{10}$$

Taking the bounce average yields a factor $1/\omega$ from the delta function. We see that for a fixed shape of the magnetic well and plasma-source boundary condition g_s, the steady-state form of f' is determined as a function of the parameters $\chi_\ell = \epsilon_\ell^2/n_s\omega$, where ϵ_ℓ is the electric field amplitude at the position where the ℓth harmonic is resonant. The χ_ℓ are convenient scaling parameters, since solutions for other values of ϵ_ℓ, n_s and ω, for the same values of χ_ℓ, then are known immediately, assuming that when the magnetic field is increased, ω is increased correspondingly.

For a low-temperature plasma source, electron trapping by second harmonic heating is much weaker than the fundamental harmonic. Strong trapping and heating of plasma source electrons should occur when RF diffusion at the fundamental harmonic is competitive with Coulomb scattering losses into the loss cone; i.e. $\nu_{RF}(\omega = \omega_c) > \nu_c/\Delta\theta^2$, where $\nu_{RF} \equiv D(\omega = \omega_c)/v^2$ is the RF velocity diffusion rate, ν_c is the 90° pitch-angle scattering frequency, and $\Delta\theta$ is the angular distance in radians to the loss cone, as shown in Fig.9. Numerically, this strong trapping condition, $\nu_{RF} > \nu_c/\Delta\theta^2$, may be written as

$$\frac{3}{2} T_s\,(\text{keV}) \gtrsim \left[\frac{n_s \times 10^{-11}\,(\text{cm}^{-3})\, f\,(\text{GHz})}{\Delta\theta^2\, \epsilon_1^2\,(\text{V/cm})}\right]^2 \tag{11}$$

At lower values of the electron temperature, T_s, Coulomb scattering will dominate RF heating so that electrons will scatter into the loss cone before their energy increases significantly.

4. PARAMETER CALCULATIONS FOR TMX-UPGRADE

Studies of hot-electron equilibria as a function of χ have been carried out for several values of plasma-source temperature neglecting ambipolar potential.

The result may be written in a conservative form

$$\left\langle\left(\frac{\partial f}{\partial t}\right)_{QL}\right\rangle = \left(\frac{1}{\tau}\right)\frac{1}{2\pi v_0^3 \sin\theta_0 \cos\theta_0} \times\left[\frac{\partial}{\partial v_0}\left(D_{vv}\frac{\partial f}{\partial v_0} + D_{v\theta}\frac{\partial f}{\partial \theta_0}\right) + \frac{\partial}{\partial \theta_0}\left(D_{v\theta}\frac{\partial f}{\partial v_0} + D_{\theta\theta}\frac{\partial f}{\partial \theta_0}\right)\right] \quad (8)$$

where the brackets denote the bounce average, $\tau = \oint ds/|v_\parallel|$ is the bounce time, and the diffusion coefficients are given by

$$D_{vv} = \oint \frac{ds}{|v_\parallel|} 2\pi\, v_0^3 \sin^3\theta_0 \cos\theta_0\, D$$

$$D_{v\theta} = \oint \frac{ds}{|v_\parallel|} 2\pi\, v_0^2 \sin^2\theta_0 \left(\frac{1 - R_\rho \sin^2\theta}{R_\rho}\right) D$$

$$D_{\theta\theta} = \oint \frac{ds}{|v_\parallel|} 2\pi\, v_0 \tan\theta_0 \left(\frac{1 - R_\rho \sin^2\theta_0}{R_\rho}\right)^2 D$$

Note that we have used a non-relativistic form of the quasi-linear equation. To include the effects of the relativistic resonance shift, we replace $\delta(\omega - \ell\omega_c)$ by $\delta(\omega - \ell\omega_c/\gamma)$ in Eq.(7), where γ is the mass factor defined earlier. Then, the Fokker-Planck equation to be solved is

$$\frac{\partial f}{\partial t} = \left\langle\left(\frac{\partial f}{\partial t}\right)_{cc}\right\rangle + \left\langle\left(\frac{\partial f}{\partial t}\right)_{QL}\right\rangle \quad (9)$$

where $\langle(\partial f/\partial t)_{cc}\rangle$ represents the bounce-averaged form of the non-linear Coulomb collision terms [13]. The boundary conditions employed are $f(v_0, \theta_{\ell c}, t) = n_s g_s(v_0)$ (i.e. fixed by a plasma source at the loss-cone boundary $\theta_0 = \theta_{\ell c}$; $f(v_{max}, \theta_0, t) = 0$ (i.e. absorbing boundary at $v = v_{max}$, normally taking the velocity of light as v_{max}); and $f(v_0, \pi/2, t)$ being regular).

Defining $f(v,\theta) \equiv n_s f'(v, \theta, t)$ we note that for the non-linear collision term $(\partial f/\partial t)_{cc} = n_s^2 (\partial f'/\partial t)_{cc}$. Performing the bounce average, the steady-state equation can be formally written as

$$0 = \pi \frac{e}{2m} \sum_\ell^2 \frac{\epsilon_\ell^2}{n_s} \left\langle \frac{1}{v_\perp}\frac{\partial}{\partial v_\perp} \times\left[v_\perp \delta\left(\omega - \frac{\ell\omega_c}{\gamma}\right) J_{\ell-1}^2\right] \frac{\partial f'}{\partial v_\perp}\right\rangle - \left\langle\left(\frac{\partial f'}{\partial t}\right)_{cc}\right\rangle \quad (10)$$

Taking the bounce average yields a factor $1/\omega$ from the delta function. We see that for a fixed shape of the magnetic well and plasma-source boundary condition g_s, the steady-state form of f' is determined as a function of the parameters $\chi_\ell = \epsilon_\ell^2/n_s\omega$, where ϵ_ℓ is the electric field amplitude at the position where the ℓth harmonic is resonant. The χ_ℓ are convenient scaling parameters, since solutions for other values of ϵ_ℓ, n_s and ω, for the same values of χ_ℓ, then are known immediately, assuming that when the magnetic field is increased, ω is increased correspondingly.

For a low-temperature plasma source, electron trapping by second harmonic heating is much weaker than the fundamental harmonic. Strong trapping and heating of plasma source electrons should occur when RF diffusion at the fundamental harmonic is competitive with Coulomb scattering losses into the loss cone; i.e. $\nu_{RF}(\omega = \omega_c) > \nu_c/\Delta\theta^2$, where $\nu_{RF} \equiv D(\omega = \omega_c)/v^2$ is the RF velocity diffusion rate, ν_c is the 90° pitch-angle scattering frequency, and $\Delta\theta$ is the angular distance in radians to the loss cone, as shown in Fig.9. Numerically, this strong trapping condition, $\nu_{RF} > \nu_c/\Delta\theta^2$, may be written as

$$\frac{3}{2} T_s\ (\mathrm{keV}) \lesssim \left[\frac{n_s \times 10^{-11}\ (\mathrm{cm}^{-3})\ f\ (\mathrm{GHz})}{\Delta\theta^2\ \epsilon_1^2\ (\mathrm{V/cm})}\right]^2 \quad (11)$$

At lower values of the electron temperature, T_s, Coulomb scattering will dominate RF heating so that electrons will scatter into the loss cone before their energy increases significantly.

4. PARAMETER CALCULATIONS FOR TMX-UPGRADE

Studies of hot-electron equilibria as a function of χ have been carried out for several values of plasma-source temperature neglecting ambipolar potential.

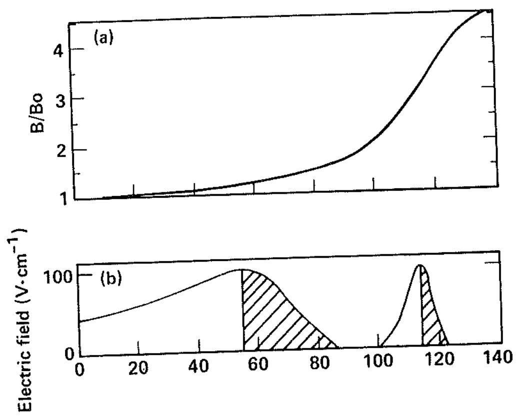

FIG.10. Axial plots of (a) magnetic field and (b) RF electric field assumed for the calculations. For $N_{\parallel} = 0$, only the shaded areas contribute to heating.

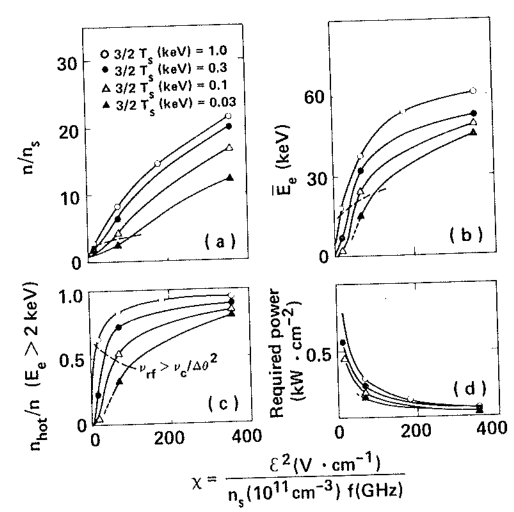

FIG.11. Plots of (a) plasma density, (b) mean electron energy, (c) fraction of hot electrons, and (d) required ECRH power as a function of χ with relativistic detuning. The parameter for the curves is plasma source energy 3/2 T_s. Plasma potential is assumed zero.

The TMX-Upgrade vacuum magnetic geometry of Fig.10 was used. The assumed RF electric fields were 100 V · cm^{-1} and the index $N_\perp = 1$ at both fundamental and second harmonic resonance.

The RF electric field is an input parameter for the calculation. A value of 100 V · cm^{-1} produces hot-electron density and energy as needed for TMX-Upgrade. Although this field value is not determined self-consistently, the hot-electron losses determined from the calculation are consistent with the available microwave power. The microwave absorption is expected to be strong, as predicted for Maxwellian plasmas. The localized heating, which limits the energy, should adjust the absorption coefficient, as manifest in the distortion of the electron velocity distribution, so that absorption and electron losses are in balance.

Calculations for heating with the fundamental and second harmonic resonance at a mirror ratio of $R_\mu = 2.3$ were carried out. The spatial variation of the RF field for the calculation approximates the beam profile in the experiment (Fig.10). Because of relativistic detuning, this results in a factor-of-10 decrease from the peak RF power at resonance for an energy $E_{10} = 63$ keV.

The variation with χ of density, mean energy, required RF power, and the fraction of hot electrons is shown in Fig.11 (a to d). The hot-electron fraction is defined as the number of electrons with energies exceeding 2 keV, the approximate depth of the thermal barrier expected in the TMX-Upgrade experiment. Electrons with lower energy would be expelled by the potential.

The plasma energy and density are seen to be increasing functions of χ and plasma-source temperature, as expected, since RF diffusion becomes relatively stronger compared with collisional losses.

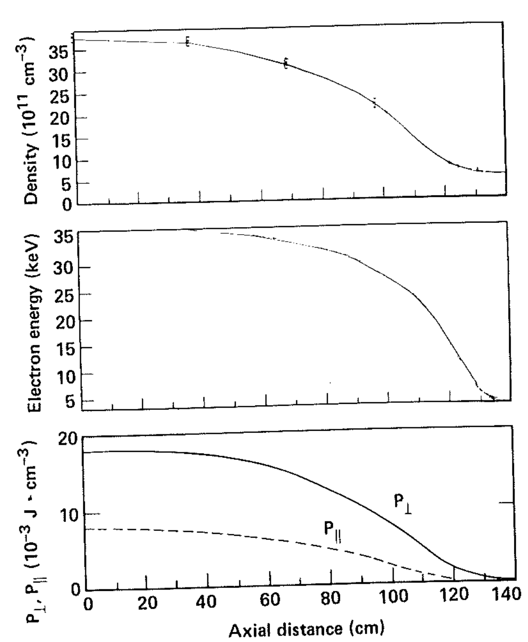

FIG.12. Calculated axial profiles of density, mean electron energy and plasma pressure for TMX-Upgrade. Plasma source conditions are $n_s = 5 \times 10^{11}$ cm^{-3} and 3/2 $T_s = 0.6$ keV.

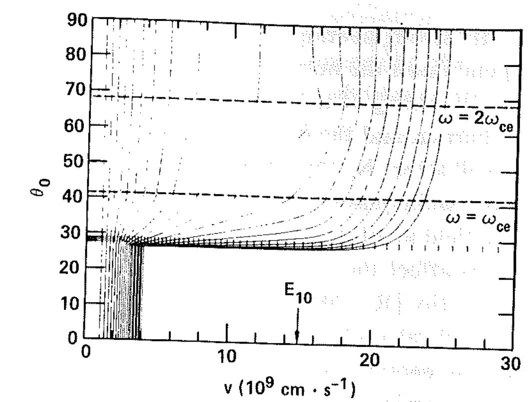

FIG.13. Contour plot of the distribution function in midplane phase space. The distribution function decreases by a factor of 0.58 between the contours.

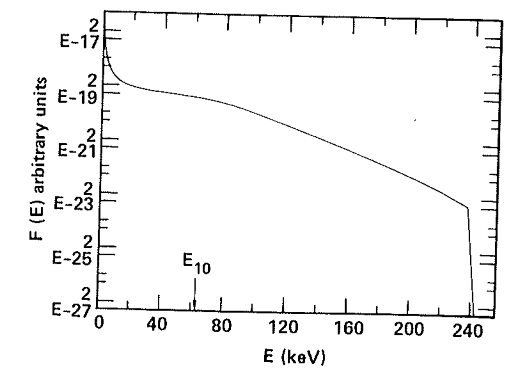

FIG.14. Energy distribution function F(E) at the midplane.

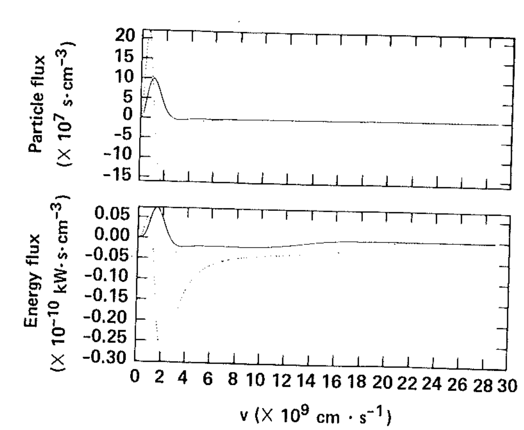

FIG.15. Electron current and energy fluxes out of one end across the loss-cone boundary due to RF diffusion (solid) and collisions (dotted). Negative fluxes refer to flow out of the trapped space.

The saturation in mean electron energy shown in Fig.11(b) results from the relativistic detuning of the RF diffusion. The dashed curves are a plot of the strong trapping condition given by Eq.(11).

An example calculation for plasma-source parameters, $n_s = 5 \times 10^{11}$ cm^{-3} and $T_s = 400$ eV, is shown in Figs 12 to 15. Figure 12 shows the axial profiles of density, mean electron energy, and parallel and perpendicular plasma pressure. Contour plots of the steady-state distribution function $f(v_0, \theta_0)$ at the midplane are shown in Fig.13. At moderate energies, f is distorted along the resonant heating lines. At higher energy, where the RF diffusion is reduced because of the relativistic detuning, the contours are weak functions of θ_0, since Coulomb collisions are the dominant processes. The same distribution function, integrated over the pitch angle θ_0, is plotted as a function of energy in Fig.14. The distribution is clearly non-Maxwellian. The stream component is visible at low energy. A break in the curve at an energy near $E_{10} = 63$ keV shows the effect of the relativistic detuning.

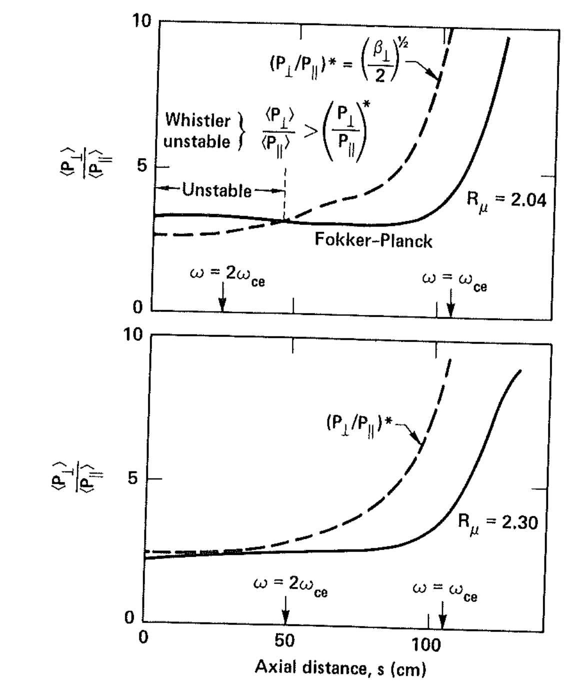

FIG.16. Plots of plasma pressure anisotropy as a function of s in the magnetic well, for several heating mirror ratios. Anisotropy increases as the mirror ratio for second harmonic heating decreases from 1.15 to 1.02. The region for Whistler instability is shown for plasma parameters scaled to $n_0 = 4 \times 10^{12}$ cm^{-3} and $E_h = 50$ keV.

The saturation in mean electron energy shown in Fig.11(b) results from the relativistic detuning of the RF diffusion. The dashed curves are a plot of the strong trapping condition given by Eq.(11).

An example calculation for plasma-source parameters, $n_s = 5 \times 10^{11}$ cm^{-3} and $T_s = 400$ eV, is shown in Figs 12 to 15. Figure 12 shows the axial profiles of density, mean electron energy, and parallel and perpendicular plasma pressure. Contour plots of the steady-state distribution function $f(v_0, \theta_0)$ at the midplane are shown in Fig.13. At moderate energies, f is distorted along the resonant heating lines. At higher energy, where the RF diffusion is reduced because of the relativistic detuning, the contours are weak functions of θ_0, since Coulomb collisions are the dominant processes. The same distribution function, integrated over the pitch angle θ_0, is plotted as a function of energy in Fig.14. The distribution is clearly non-Maxwellian. The stream component is visible at low energy. A break in the curve at an energy near $E_{10} = 63$ keV shows the effect of the relativistic detuning.

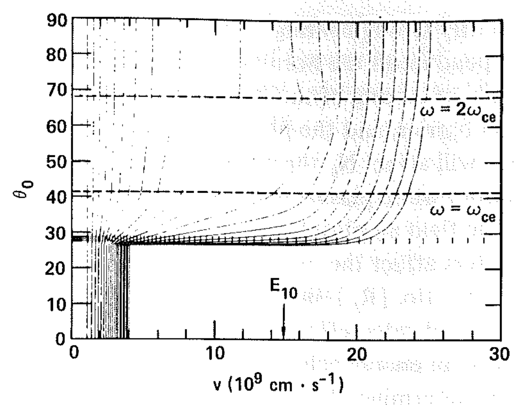

FIG.13. Contour plot of the distribution function in midplane phase space. The distribution function decreases by a factor of 0.58 between the contours.

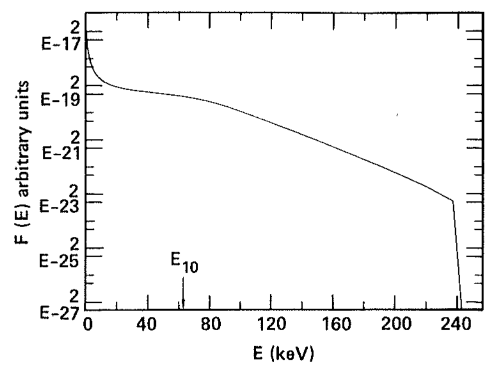

FIG.14. Energy distribution function F(E) at the midplane.

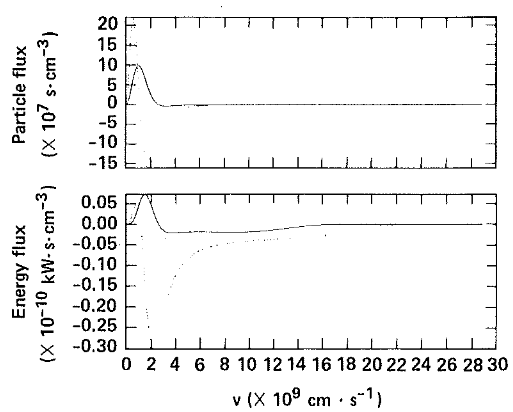

FIG.15. Electron current and energy fluxes out of one end across the loss-cone boundary due to RF diffusion (solid) and collisions (dotted). Negative fluxes refer to flow out of the trapped space.

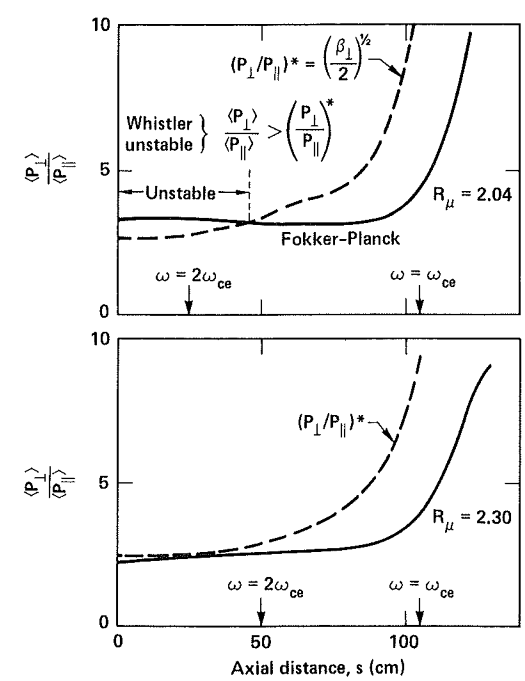

FIG.16. Plots of plasma pressure anisotropy as a function of s in the magnetic well, for several heating mirror ratios. Anisotropy increases as the mirror ratio for second harmonic heating decreases from 1.15 to 1.02. The region for Whistler instability is shown for plasma parameters scaled to $n_0 = 4 \times 10^{12}$ cm^{-3} and $E_h = 50$ keV.

The current and power fluxes across the loss-cone boundary due to collisions (dotted curves) and RF diffusion (solid curves) are shown in Fig.15. For this example the dominant current flow is at low energy. A cold electron initially trapped by ECRH near the loss cone has a small probability of reaching high energy compared with the probability of loss during heating. Consequently, the overall particle balance is determined at low energy, $E \sim T_s$.

On the other hand, the major component of power flow occurs at higher energy. For parameters such that $n_h/n_c \gg 1$, the required RF power can be roughly estimated from the collisional and diffusion losses of the hot electrons.

The sensitivity of the hot-electron anisotropy to the mirror ratio for heating is shown in Fig.16 for energy detuning E_{10} held constant. The axial variation of $P_\perp/P_\parallel$ for thermal-barrier heating near the bottom of the well at $R_\mu = 2.04$ is compared with the similar plot for $R_\mu = 2.3$. The anisotropy increases from 2.3 to 3.3 as R_μ decreases from 2.3 to 2.04. Also indicated in the figure is the stability boundary for the anisotropy-driven Whistler instability. If $P_\perp/P_\parallel$ is below the stability boundary, Whistler waves are stable, as shown in Fig.16(b). This formula, derived by Hedrick, is given in Ref.[8]. Apparently, instability can exist near the well bottom if R_μ becomes too small, as in Fig.16(a).

5. SUMMARY

The Fokker-Planck model has demonstrated the sensitivity of the hot-electron component to the parameter χ. At small values of χ, the hot-to-cold density ratio is small ($n_h/n_c < 1$), which is characteristic of the regime for devices like EBT with electric field $\epsilon < 10\ \mathrm{V \cdot cm^{-1}}$. We would not expect the code to predict EBT parameters since the equations are non-relativistic and, in addition, higher harmonics than $\ell = 2$, which are believed to be important for heating in EBT [14], are not included. Nevertheless, the curves seem qualitatively correct. As χ increases at higher power levels, we reach the tandem-mirror density regime for thermal-barrier devices ($n_h/n_c \gg 1$). The efficiency of fuelling the hot-electron population from the cold-stream population, which increases with χ, is the dominant process.

For TMX-Upgrade the assumptions of the Fokker-Planck model are a reasonable first approximation. The results indicate that the desired parameters of hot-electron energy and density may be achieved with sufficiently strong heating. The hot-electron energy will depend upon the horn placement along the axis, the angle of aiming of the microwave horns in the thermal barrier, and the plasma density. Plasma density will affect $N_\parallel$ through ray bending due to refraction, while plasma beta will reduce the local magnetic field amplitude and scale length. These parameters affect the magnitude of $N_\parallel$ and the range of mirror ratio, $[R_\rho]$, illuminated by the antennae. These complicated effects will determine the actual hot-electron energy achieved. The optimum conditions must be determined by experiment.

Localized heating appears necessary in order to limit hot-electron runaway. The resonance plots shown in Figs 6 and 8 suggest that cavity heating, as employed in devices like EBT (RF at all values of magnetic field and a broad spectrum of $N_\parallel$), should lead to much higher energy since higher harmonics are accessible. The plasma beta is then created by a relatively low density of very energetic electrons, in contrast to the higher density and lower energy desired for thermal barriers.

Important results of localized heating are (1) hot-electron populations with significant density extending to large mirror ratio and (2) only moderate energy anisotropy. These results are a consequence of small-angle scattering into the loss cone as the particle loss process. We may speculate that the non-adiabatic loss process observed in experiments with cavity heating will lead to relatively shorter hot-electron populations with larger anisotropy ($P_\perp/P_\parallel$), as has been observed [15]. With cavity heating, electrons would reach the non-adiabatic energy-loss boundary at large pitch angle, then rapidly angle-scatter into the loss cone, thereby contributing little density at large mirror ratios.

Limitations of the present calculations, in addition to the assumption $N_\parallel = 0$, as well as the incomplete treatment of relativity in the equations of motion, include the neglect of plasma potential. Potentials, if comparable to the plasma-stream energy, can significantly affect the density of cold plasma at the fundamental resonance. The feed of the hot-electron population, in turn, can be affected. The inclusion of all these effects is under way in our ongoing code development work.

ACKNOWLEDGEMENTS

The authors wish to thank L. Friedland, M. Porkolab and T.D. Rognlien for their valuable assistance and discussions during this work.

This work was performed under the auspices of the United States Department of Energy by the Lawrence Livermore National Laboratory under Contract No. W-7405-ENG-48.

REFERENCES

[1] BALDWIN, D.E., LOGAN, B.G., Phys. Rev. Lett. **43** (1979) 1318.

[2] DIMOV, G.I., ZAKAIDAKOV, V.V., KISHINEVSKIJ, M.E., Fiz. Plazmy 2 (1976) 597 (Sov. J. Plasma Phys. **2** (1976) 326).
FOWLER, T.K., LOGAN, B.G., Comments Plasma Phys. Controll. Fus. 2 (1977) 167.
CORRELL, D.L., ALLEN, S.L., CASPER, T.A., CLAUSER, J.F., COAKLEY, P., COENSGEN, F.H., CONDIT, W., CUMMINS, W.F., DAVIS, J.C., DRAKE, R.P., FOOTE, J.H., FUTCH, A.H., GOODMAN, R.K., GRUBB, D.P., HALLOCK, G.A., HOOPER, E.B., HORNADY, R.S., HUNT, A.L., KARMENDY, C.V., MOLVIK, A.W., NEXSEN, W.E., PICKLES, W.L., POULSEN, P., SIMONEN, T.C., STALLARD, B.W., STRAND, O.T., Nucl. Fusion **22** (1982) 223.

[3] COHEN, R.H., BERNSTEIN, I.B., DORNING, J.J., ROWLANDS, G., Nucl. Fusion **20** (1980) 1421.

[4] COENSGEN, F.H., et al., TMX Upgrade Major Project Proposal, Lawrence Livermore National Laboratory, Livermore, CA, Rep. LLL-Prop-172 (1980).
COENSGEN, F.H., et al., Proc. Workshop on Ambipolar Potential Formation and Control in Bumpy Torus and Mirrors, Oak Ridge, TN (1981) 381.

[5] DANDL, R.A., ENGLAND, A.C., ARD, W.B., EASON, H.O., BERBER, M.C., HAAS, G.M., Nucl. Fusion 4 (1964) 344.
ARD, W.B., BLANKEN, R.A., COLCHIN, R.J., DUNLAP, J.L., GUEST, G.E., HASTE, G.L., HEDRICK, C.L., LAZAR, N.H., LYON, J.F., SIGMAR, D.J., Plasma Physics and Controlled Nuclear Fusion Research – 1971 (Proc. 4th Conf. Madison, 1971) Vol.2, IAEA, Vienna (1971) 619.
DANDL, R.A., EASON, H.O., GUEST, G.E., HEDRICK, C.C., IKEGAMI, H., NELSON, D.B., Plasma Physics and Controlled Nuclear Fusion Research – 1974 (Proc. 5th Conf. Tokyo, 1974) Vol.2, IAEA, Vienna (1975) 141.
IKEGAMI, H., AIHARA, S., HOSOKAWA, M., AIKAWA, H., Nucl. Fusion **13** (1973) 351.

[6] UCKAN, N.A., Bull. Am. Phys. Soc. **26** (1981) 994 (also to be published in Phys. Fluids).

[7] NEWCOMB, W.A., J. Plasma Phys. **26** (1981) 529.

[8] GUEST, G.E., SIGMAR, D.J., Nucl. Fusion **11** (1971) 151.

[9] ANTONSEN, T.M., Jr., MANHEIMER, W.M., Phys. Fluids **21** (1978) 2295.
PORKOLAB, M., FRIEDLAND, L., BERNSTEIN, I.B., Nucl. Fusion **21** (1981) 1643.
HUI, B., CHU, K.R., OTT, E., ANTONSEN, T., Phys. Fluids **23** (1980) 822.

[10] BATCHELOR, D.B., GOLDFINGER, R.C., WEITZNER, H., IEEE Trans. Plasma Sci. PS-8 (1980) 78.

[11] FIDONE, I., GRANATA, G., RAMPONI, G., MEYER, R.C., Phys. Fluids **21** (1978) 645.
BORNATICI, M., ENGLEMANN, F., LISTA, G.G., Phys. Fluids **22** (1979) 1664.

[12] ROGNLIEN, T.D., private communication, April 1982.

[13] CUTLER, T.A., PEARLSTEIN, L.D., RENSINK, M.E., Computation of the Bounce Average Code, Lawrence Livermore National Laboratory, Livermore, CA, Rep. UCRL-52233 (1977).

[14] BATCHELOR, D.B., GOLDFINGER, R.C., WEITZNER, H., Bull. Am. Phys. Soc. **25** (1980) 964.

[15] LAO, L.N., QUON, B.H., DANDL, R.A., GUEST, G.E., LAZAR, N.H., SAMEC, T.K., Bull. Am. Phys. Soc. **26** (1981) 928.

(Manuscript received 21 July 1982
Final manuscript received 25 November 1982)

This work was performed under the auspices of the United States Department of Energy by the Lawrence Livermore National Laboratory under Contract No. W-7405-ENG-48.

REFERENCES

[1] BALDWIN, D.E., LOGAN, B.G., Phys. Rev. Lett. **43** (1979) 1318.

[2] DIMOV, G.I., ZAKAIDAKOV, V.V., KISHINEVSKIJ,M.E., Fiz. Plazmy 2 (1976) 597 (Sov. J. Plasma Phys. **2** (1976) 326).
FOWLER, T.K., LOGAN, B.G., Comments Plasma Phys. Controll. Fus. 2 (1977) 167.
CORRELL, D.L., ALLEN, S.L., CASPER, T.A., CLAUSER, J.F., COAKLEY, P., COENSGEN, F.H., CONDIT, W., CUMMINS, W.F., DAVIS, J.C., DRAKE, R.P., FOOTE, J.H., FUTCH, A.H., GOODMAN, R.K., GRUBB, D.P., HALLOCK, G.A., HOOPER, E.B., HORNADY, R.S., HUNT, A.L., KARMENDY, C.V., MOLVIK, A.W., NEXSEN, W.E., PICKLES, W.L., POULSEN, P., SIMONEN, T.C., STALLARD, B.W., STRAND, O.T., Nucl. Fusion **22** (1982) 223.

[3] COHEN, R.H., BERNSTEIN, I.B., DORNING, J.J., ROWLANDS, G., Nucl. Fusion **20** (1980) 1421.

[4] COENSGEN, F.H., et al., TMX Upgrade Major Project Proposal, Lawrence Livermore National Laboratory, Livermore, CA, Rep. LLL-Prop-172 (1980).
COENSGEN, F.H., et al., Proc. Workshop on Ambipolar Potential Formation and Control in Bumpy Torus and Mirrors, Oak Ridge, TN (1981) 381.

[5] DANDL, R.A., ENGLAND, A.C., ARD, W.B., EASON, H.O., BERBER, M.C., HAAS, G.M., Nucl. Fusion **4** (1964) 344.
ARD, W.B., BLANKEN, R.A., COLCHIN, R.J., DUNLAP, J.L., GUEST, G.E., HASTE, G.L., HEDRICK, C.L., LAZAR, N.H., LYON, J.F., SIGMAR, D.J., Plasma Physics and Controlled Nuclear Fusion Research – 1971 (Proc. 4th Conf. Madison, 1971) Vol.2, IAEA, Vienna (1971) 619.
DANDL, R.A., EASON, H.O., GUEST, G.E., HEDRICK, C.C., IKEGAMI, H., NELSON, D.B., Plasma Physics and Controlled Nuclear Fusion Research – 1974 (Proc. 5th Conf. Tokyo, 1974) Vol.2, IAEA, Vienna (1975) 141.
IKEGAMI, H., AIHARA, S., HOSOKAWA, M., AIKAWA, H., Nucl. Fusion **13** (1973) 351.

[6] UCKAN, N.A., Bull. Am. Phys. Soc. **26** (1981) 994 (also to be published in Phys. Fluids).

[7] NEWCOMB, W.A., J. Plasma Phys. **26** (1981) 529.

[8] GUEST, G.E., SIGMAR, D.J., Nucl. Fusion **11** (1971) 151.

[9] ANTONSEN, T.M., Jr., MANHEIMER, W.M., Phys. Fluids **21** (1978) 2295.
PORKOLAB, M., FRIEDLAND, L., BERNSTEIN, I.B., Nucl. Fusion **21** (1981) 1643.
HUI, B., CHU, K.R., OTT, E., ANTONSEN, T., Phys. Fluids **23** (1980) 822.

[10] BATCHELOR, D.B., GOLDFINGER, R.C., WEITZNER, H., IEEE Trans. Plasma Sci. PS-8 (1980) 78.

[11] FIDONE, I., GRANATA, G., RAMPONI, G., MEYER, R.C., Phys. Fluids **21** (1978) 645.
BORNATICI, M., ENGLEMANN, F., LISTA, G.G., Phys. Fluids **22** (1979) 1664.

[12] ROGNLIEN, T.D., private communication, April 1982.

[13] CUTLER, T.A., PEARLSTEIN, L.D., RENSINK, M.E., Computation of the Bounce Average Code, Lawrence Livermore National Laboratory, Livermore, CA, Rep. UCRL-52233 (1977).

[14] BATCHELOR, D.B., GOLDFINGER, R.C., WEITZNER, H., Bull. Am. Phys. Soc. **25** (1980) 964.

[15] LAO, L.N., QUON, B.H., DANDL, R.A., GUEST, G.E., LAZAR, N.H., SAMEC, T.K., Bull. Am. Phys. Soc. **26** (1981) 928.

(Manuscript received 21 July 1982
Final manuscript received 25 November 1982)